Catalysis Today 147S (2009) S250–S256

Contents lists available at ScienceDirect

Catalysis Today

journal homepage: www.elsevier.com/locate/cattod

A global kinetic model for NO_x storage and reduction on $Pt/BaO/Al_2O_3$ monolithic catalysts

Divesh Bhatia [a], Robert D. Clayton [b], Michael P. Harold [a,*], Vemuri Balakotaiah [a,*]

[a] Department of Chemical & Biomolecular Engineering, University of Houston, Houston, TX, United States
[b] Caterpillar Inc., Peoria, IL, United States

ARTICLE INFO

Article history:
Available online 4 August 2009

Keywords:
NO_x storage and reduction
NO_x trap
Monolith
LNT modeling
Kinetics

ABSTRACT

A global kinetic model for NO_x storage and reduction for the case of anaerobic regeneration with hydrogen is developed, based on parallel experimental studies [R.D. Clayton, M.P. Harold, V. Balakotaiah, Appl. Catal., B 84 (2008) 616; R.D. Clayton, M.P. Harold, V. Balakotaiah, C.Z. Wan, Appl. Catal., B 90 (2009) 662.]. The existence of two different types of BaO storage sites on the catalyst is proposed, which differ in their storage as well as regeneration activity. The two-site model explains the close to complete NO_x storage at the start of the storage phase and the gradual emergence of NO and NO_2 during later storage times. The effluent concentrations and concentration fronts of the reactants and products within the monolith are predicted by the model, providing insight into the mechanisms of regeneration and storage. The H_2 front velocities are predicted to increase as the H_2 front propagates down the length of the monolith, thus showing the presence of more stored NO_x in the front of the reactor. The simulations show that even though regeneration is fast, H_2 concentration fronts are not very steep, which is attributed to the lower regeneration activity of the "slow" sites. The model captures the formation of NH_3 and the NH_3 concentration fronts, which reveal the reaction of NH_3 formed upstream with the stored NO_x downstream of the H_2 front. The lower diffusivity of NH_3 as compared to H_2 is shown to be responsible for the wider width of the NH_3 front and earlier appearance of NH_3 in the effluent than H_2.

1. Introduction

The storage and reduction of nitrogen oxides (or NO_x) has emerged as a commercially viable technology for lean burn gasoline and light duty diesel vehicles. NO_x storage and reduction (NSR) is a complex process carried out in a monolith reactor containing a multi-functional catalyst. Its operation involves the sequential trapping of NO_x on an alkaline earth oxide, followed by reduction of the stored NO_x species. Both the storage and regeneration steps involve traveling concentration fronts. During storage, a front of stored NO_x moves through the monolith as uptake occurs with a gradual emergence of NO and NO_2. During regeneration, a front comprising the reductant(s) has a rather sharp breakthrough at temperatures above 250 °C, occurring once most of the stored NO_x has been regenerated [1,3].

A number of lean NO_x trap models of varying complexity have been developed in concert with key experimental studies. A survey has been provided by Guthenke et al. [4], a few of the more recent ones of which will be summarized here. Sharma et al. [5] developed a LNT model with propylene as the reductant and used Langmuir adsorption kinetics for the NO_x trapping. This model was upgraded by Sharma et al. [6] using a NO_x storage model developed earlier [7]. A simpler description of the storage process assumes the existence of fast and slow sites, respectively corresponding to the storage sites in close proximity to the precious metal sites and others further removed [8–11]. Tuttlies et al. [12] developed a model for the NO/CO system which considered diffusion limitations brought about by density changes during nitration of barium carbonate particles. Olsson et al. [13] followed with a global model which described the NO_x storage process with a shrinking core storage phase. Koci et al. [14] developed LNT models containing global kinetics for a large number of reactions, although the parameter values were not provided. It was shown that ammonia serves as a hydrogen carrier which readily reacts with the stored NO_x [15,16]. The reduction was found to be transport limited and therefore the reduction kinetics or the identity of the reductant was reported to be unimportant [3]. Clayton et al. [1] showed that kinetic effects emerge at lower temperatures due to reactivity differences between H_2 and NH_3. Lietti et al. [17] showed further evidence of the intermediate role of ammonia, while Clayton et al. [2] have shown interesting effects of the Pt dispersion on the net formation of ammonia. Finally, Larson

* Corresponding authors.
E-mail addresses: Clayton_Robert_D@cat.com (R.D. Clayton), mharold@uh.edu (M.P. Harold), bala@uh.edu (V. Balakotaiah).

0920-5861/$ – see front matter © 2009 Elsevier B.V. All rights reserved.
doi:10.1016/j.cattod.2009.07.024

Nomenclature

A_{i2}	pre-exponential factors for NO oxidation reaction (mol/m^3 washcoat s)
c_{BaO}	concentration of exposed BaO sites (mol/m^3 washcoat)
c_{Tm}	total molar concentration (mol/m^3)
c_X	concentration of adsorption sites for H_2O and NH_3 (mol/m^3 washcoat)
D_{jm}	diffusivity of species j in the gas phase (m^2/s)
$k_c(j, z)$	mass transfer coefficient of species j at axial position z (m/s)
k_i	rate constant for reaction i (s^{-1})
L	length of the monolith sample (m)
rxn	number of reactions
$R_{ad,j}$	adsorption rate of gaseous species j (mol/m^3 washcoat s)
$R_{des,j}$	desorption rate of gaseous species j (mol/m^3 washcoat s)
$R_{v,l}$	rate of reaction l (mol/m^3 washcoat s)
R_Ω	effective transverse length scale (m)
$\bar{u}$	average gas velocity in the gas phase (m/s)
X_{jm}	dimensionless cup-mixing concentration of species j in fluid
$X_{j,wc}$	dimensionless concentration of species j at fluid–washcoat interface

Greek letters

δ_c	washcoat thickness (m)
ε_{wc}	porosity of the washcoat
$\theta_{Ba(NO_3)_2}$	fractional surface coverage of barium sites occupied by NO_x
$\theta_{j,X}$	fractional surface coverage of species j on adsorption sites X
θ_v	fractional surface coverage of vacant sites on barium
$\theta_{v,X}$	fractional surface coverage of vacant sites on adsorption sites X
ϑ_{lj}	stoichiometric coefficient of species j in reaction l (negative for reactant)

et al. [18] incorporated a microkinetic model into a monolith model to simulate the steady-state NO_x reduction by H_2 and CO in the presence of O_2. Xu et al. [19] provided a microkinetic framework model of steady-state NO reduction by H_2 in the presence of O_2 in a monolith reactor. Lindholm et al. [20] developed a LNT reactor model containing a microkinetic description of the NO_x storage and reduction chemistry.

The objective of the current study is to develop an integral monolith reactor model that incorporates global kinetics for the storage and reduction. We show that a relatively simple description of the NO_x uptake and regeneration by H_2 is sufficient to capture the main spatio-temporal features of the lean NO_x trap reported by Clayton et al. [1,2].

2. Model development

A one-dimensional two-phase transient model is used to predict the spatio-temporal concentration profiles. The model equations consist of species balances in the fluid and solid phase and are given in Table 1. The energy balance equations are not incorporated in the current model because of the near isothermal conditions in the experiments reported by Clayton et al. [1]. Position dependent mass transfer coefficients are evaluated for a channel of square cross-section to account for the transverse gradients following Ramanathan et al. [21]. The following assumptions are made: (i) constant physical properties and (ii) laminar flow. Any possible effects of washcoat diffusion are incorporated in the values of the estimated kinetic parameters. For details on the evaluation of certain parameters like R_Ω, D_{jm}, etc., please refer Bhatia et al. [22]. The values of physical properties and other parameters used in the simulations are given in Table 2.

Table 1
One-dimensional two-phase model equations.

$$\frac{\partial X_{jm}}{\partial t} = -\bar{u}\frac{\partial X_{jm}}{\partial z} - \frac{k_c(j,z)}{R_\Omega}(X_{jm} - X_{j,wc})$$

$$\varepsilon_{wc}\frac{\partial X_{j,wc}}{\partial t} = \frac{k_c(j,z)}{\delta_c}(X_{jm} - X_{j,wc}) + \frac{1}{c_{Tm}}\left(\sum_{l=1}^{rxn}[\vartheta_{lj}R_{v,l}(\underline{\theta}, \underline{X}_{wc})] - R_{ad,j} + R_{des,j}\right)$$

$$c_{BaO}(f,s)\frac{\partial \theta_{v(f,s)}}{\partial t} = \sum_{l=1}^{rxn}\vartheta_{l,BaO(f,s)}R_{v,l}(\underline{\theta}, \underline{X}_{wc}); \qquad c_X\frac{\partial \theta_{j,X}}{\partial t} = R_{ad,j} - R_{des,j}$$

Boundary conditions : $X_{jm} = X_{jm,in}$ @ $z = 0$

Initial conditions : $X_{jm} = 0$, $X_{j,wc} = 0$, $\theta_j = \theta_{jo}$ @ $t = 0$

The experiments which were used to develop the kinetic model were carried out over a reduced $Pt/BaO/Al_2O_3$ catalyst at an inlet feed temperature of 275 °C [1]. The experiments consisted of flowing 500 ppm NO and 5% O_2 for 60 s during the lean phase, and 1500 ppm H_2 for 60 s in the absence of O_2 during the rich phase, until a pseudo-steady state was attained. The length of the monolith piece was 2 cm and the space velocity was 60 000 h^{-1}. For the construction of spatio-temporal concentration profiles, the experiments were replicated for a series of monoliths of progressively decreasing lengths.

The lean NO_x trap (LNT) catalyst readily stores NO_2 as compared to NO [8,23]. For this reason, NO should be oxidized to NO_2 to achieve an acceptable level of NO_x storage. Hence, we consider the oxidation of NO in the storage model, the global kinetics of which have been obtained from Bhatia et al. [24]. It has been reported in the literature that NO_2 storage on Pt/BaO catalysts occurs according to a disproportionation reaction [10,24,25]. Hence, in our model, the storage is proposed to occur via the sequential route: NO oxidation to produce NO_2, followed by the disproportionation reaction.

Fig. 1(a) shows the experimental effluent NO and NO_2 concentrations during the lean phase of a cycling experiment in which the regeneration is of a sufficient duration that the catalyst is fully reduced prior to the storage. It is observed that for early storage times (<ca. 25 s), NO or NO_2 are not observed in the effluent. However, after about 25 s, there is a gradual emergence of NO and NO_2 in the effluent with the NO_2 concentration slightly

Table 2
Values of parameters used in the simulations.

Parameter	Numerical value
$\bar{u}$	0.98 m/s
L	0.02 m
R_Ω	2.75×10^{-4} m
δ_c	3.0×10^{-5} m
c_{Tm}	22.2 mol/m^3
$D_{NO,m}$	5.2×10^{-5} m^2/s
$D_{O_2,m}$	5.19×10^{-5} m^2/s
$D_{NO_2,m}$	4.2×10^{-5} m^2/s
$D_{N_2,m}$	5.14×10^{-5} m^2/s
$D_{H_2,m}$	2.05×10^{-4} m^2/s
$D_{NH_3,m}$	6.9×10^{-5} m^2/s
$D_{H_2O,m}$	6.85×10^{-5} m^2/s
ε_{wc}	0.4

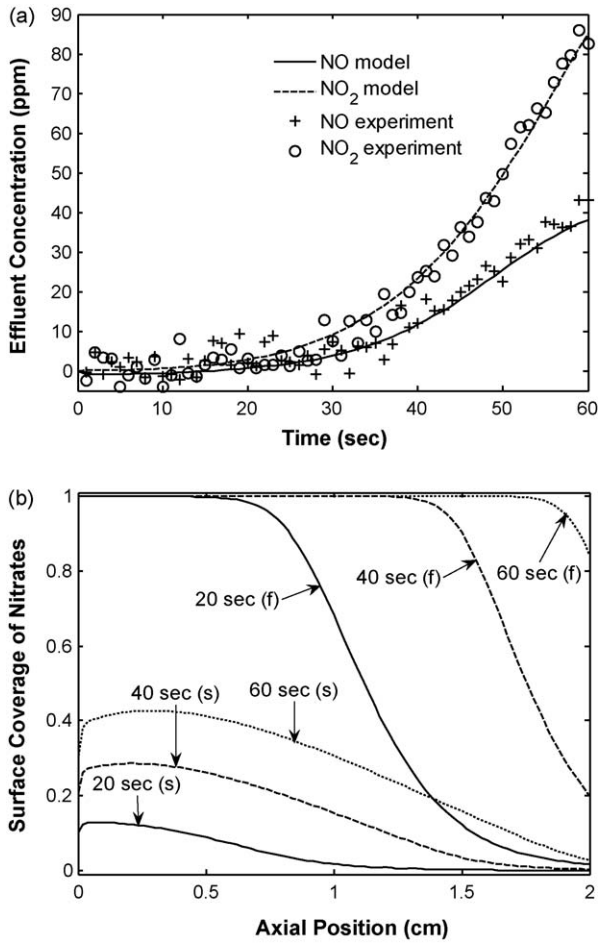

Fig. 1. (a) Comparison of model-predicted and experimental NO and NO_2 effluent concentrations during storage (inlet NO = 500 ppm; O_2 = 5%). (b) Variation of fractional surface coverage of nitrates with axial position at various times during storage ((f) and (s) denote fast and slow storage sites, respectively) (inlet NO = 500 ppm; O_2 = 5%).

exceeding that of NO. To predict these trends, we assume the presence of two different storage sites, which differ in their capacity to store NO_x and in the rate at which NO_x is stored. The presence of two different storage sites was proposed by Kromer et al. [11]. The "fast" storage sites are conjectured to be in close proximity to the Pt/BaO interface and involve spillover processes; these are used to predict the early storage data during which there is no evolution of NO or NO_2. This is in contrast to the "slow" sites, which are presumably further away from the Pt sites and are more likely to involve gas phase transport; these are used to predict the gradual increase of NO and NO_2 effluent concentrations with time. The global reactions used to model the storage are as follows:

$$1.\quad NO + \tfrac{1}{2}O_2 \overset{Pt}{\longleftrightarrow} NO_2 \tag{2.1}$$

$$2.\quad 3NO_2 + BaO(f) \rightarrow Ba(NO_3)_2(f) + NO \tag{2.2}$$

$$3.\quad 3NO_2 + BaO(s) \rightarrow Ba(NO_3)_2(s) + NO \tag{2.3}$$

The corresponding rate expressions for the above reactions are given by

$$R_{v1} = k_{f2} X_{O_2,wc} \left[1 - \left(\frac{X_{NO_2,wc}}{K_{eq}\sqrt{X_{O_2,wc}} X_{NO,wc}}\right)^2\right] \times \frac{1}{K_1 X_{NO,wc} + (1/K_3)(K_4 X_{NO_2,wc}/K_1 X_{NO,wc})} \tag{2.4}$$

Table 3
Parameter values used in the storage simulations.

Parameter	Numerical value
$c_{BaO}(f)$	6.62×10^1 mol/m^3 washcoat
$c_{BaO}(s)$	2.72×10^2 mol/m^3 washcoat
A_{f2}	6.81×10^4 mol/m^3 washcoat s
A_{b2}	8.41×10^{12} mol/m^3 washcoat s
k_2	4.17×10^3 s^{-1}
k_3	6.28×10^1 s^{-1}

$$R_{v2} = k_2 X_{NO_2,wc} c_{BaO}(f)\theta_v(f); \quad R_{v3} = k_3 X_{NO_2,wc} c_{BaO}(s)\theta_v(s) \tag{2.5}$$

$$\theta_v(f) + \theta_{Ba(NO_3)_2}(f) = 1; \quad \theta_v(s) + \theta_{Ba(NO_3)_2}(s) = 1 \tag{2.6}$$

The letters 'f' and 's' in parenthesis represent the fast and slow storage sites, respectively. The details of the kinetic constants in Eq. (2.4) and their values are given in another work [24]. The pre-exponential factors A_{f2} and A_{b2} (of the rate limiting step) were changed to reflect differences in the volume concentration of Pt in the washcoat arising due to the assumed washcoat thicknesses. The model equations in Table 1 along with the rate expressions given by Eqs. (2.4) and (2.5) are used to predict the effluent concentrations of NO and NO_2, assuming a completely reduced catalyst at the start of storage. The value of $c_{BaO}(f)$ is estimated by the breakthrough times for NO and NO_2 during storage, whereas the value of $c_{BaO}(s)$ is obtained using the NO_x storage capacity for longer storage times (~5 min). The values of rate constants viz., k_2 and k_3, were adjusted to predict the experimental data and are given in Table 3, along with the concentration of fast and slow barium sites.

It is observed from Fig. 1(a) that the storage model captures the effluent concentration profiles of NO and NO_2. It was attempted to explain the storage data using a single type of storage site. In doing so, when the rate constants of the storage reaction were increased, the effluent NO and NO_2 concentrations showed a steep increase with time, which is in contrast to the experimentally observed gradual increase in the concentrations. If the rate constants are decreased, the model predicts non-zero effluent NO and NO_2 concentrations, even at early storage times. It has been reported that NO_2 stores on BaO in the absence of Pt [10], and the addition of Pt increases the storage capacity and the rate of storage. Hence, the fast storage sites in our model represent the storage which occurs by the interaction between Pt and BaO, probably via a spillover mechanism. On the other hand, the slow sites represent the Ba that is removed from the Pt/BaO interface and stores NO_2 which is transported either by solid state diffusion or directly from the gas phase.

Fig. 1(b) shows the variation of fractional surface coverage of nitrates with axial position at various times during the storage. It is observed that as time progresses, most of the fast storage sites become covered by nitrates. Even though the fractional surface coverage of nitrates on the slow storage sites is relatively low, the total amount of nitrates on the fast and slow sites at the end of storage is almost the same. This is because of the higher concentration of slow storage sites, as seen in Table 3.

The cycling experiments consisted of flowing 500 ppm NO and 5% O_2 for 60 s during the lean phase, and 1500 ppm H_2 for 60 s during the rich phase, until a pseudo-steady state was attained. The effluent concentration profiles during the regeneration phase of the cycling experiment are shown in Fig. 2. It is seen that H_2 and NH_3 do not appear in the effluent until approximately 40 s into the regeneration. After 8 s into the regeneration and until the breakthrough of H_2, the effluent concentrations of H_2O and N_2 are observed to be close to 1500 and 300 ppm, respectively. The inlet H_2 and effluent H_2O concentrations (1500 ppm) indicate a 1:1

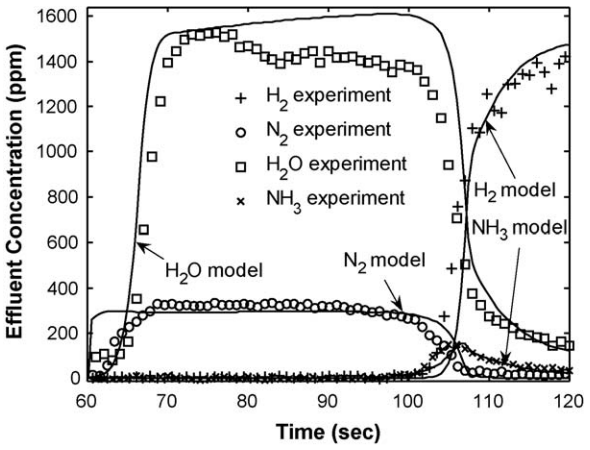

Fig. 2. Comparison of model-predicted and experimental effluent concentrations during regeneration at 275 °C (inlet H_2 = 1500 ppm).

stoichiometry between H_2O formed and H_2 consumed. Also, the effluent concentration of N_2 indicates a 1:5 stoichiometry between the moles of N_2 formed and H_2 consumed. This is consistent with the overall reaction during regeneration: $5H_2 + Ba(NO_3)_2 \rightarrow 5H_2O + BaO + N_2$ and implies that during storage, most of the NO_x is stored in the form of nitrates. The data shows that NH_3 is a product during the regeneration, and its breakthrough occurs at essentially the same time that H_2 is observed. This observation has been attributed to the reaction of NH_3 produced with stored NO_x downstream [1,3,15,16], due to which NH_3 is not observed in the effluent for early regeneration times. Once the stored NO_x gets depleted, NH_3 and H_2 are observed in the effluent. A maximum in NH_3 concentration is a result of the depletion of stored NO_x during regeneration.

It is observed from Fig. 2 that during regeneration, H_2O does not appear in the effluent for the first few seconds, even though H_2 is consumed. Also, the effluent concentrations of H_2O and NH_3 decrease gradually with time. These observations suggest the adsorption of H_2O and NH_3 on the catalyst. Also, there is a delay in the effluent N_2, which could be due to the non-availability of NH_3 formed to react with the stored NO_x. The low affinity of N_2 to the catalyst surface and its delay in the effluent indicates that the major route for N_2 production is by the reaction of NH_3 with stored NO_x. Hence, the following steps are proposed to occur:

4. $$8H_2 + Ba(NO_3)_2(f) \xrightarrow{Pt} 5H_2O + BaO(f) + 2NH_3 \quad (2.7)$$

5. $$8H_2 + Ba(NO_3)_2(s) \xrightarrow{Pt} 5H_2O + BaO(s) + 2NH_3 \quad (2.8)$$

6. $$\tfrac{10}{3}NH_3 + Ba(NO_3)_2(f) \xrightarrow{Pt} 5H_2O + BaO(f) + \tfrac{8}{3}N_2 \quad (2.9)$$

7. $$\tfrac{10}{3}NH_3 + Ba(NO_3)_2(s) \xrightarrow{Pt} 5H_2O + BaO(s) + \tfrac{8}{3}N_2 \quad (2.10)$$

8. $$H_2O + X \Leftrightarrow H_2O - X \quad (2.11)$$

9. $$NH_3 + X \Leftrightarrow NH_3 - X \quad (2.12)$$

The reactions represented by Eqs. (2.7)–(2.10) consider the Pt-catalyzed formation of NH_3 and its consumption by stored NO_x to form N_2. The integral ratio of H_2 consumed to N_2 formed was found to be 5.5, which is more than the stoichiometrically expected value of 5.0 based on the reaction of H_2 with stored nitrates to produce N_2. This suggests that some of the H_2 may be consumed by chemisorbed O on the Pt surface. An analysis showed that approximately 80% of the exposed Pt was occupied by chemisorbed O. However, the moles of H_2 consumed by chemisorbed O ($=1.7 \times 10^{-6}$) were estimated to be negligible in comparison to that consumed by stored nitrates ($=46.4 \times 10^{-6}$). Hence, the consumption of H_2 by chemisorbed O is not considered in the present model. It is assumed that H_2O and NH_3 adsorb on the catalyst and the corresponding steps are represented by Eqs. (2.11) and (2.12), respectively. Here, 'X' represents a lumped storage site to account for the adsorption of H_2O and NH_3 on Al_2O_3 and/or BaO. Since the fast sites are presumably in close proximity to the Pt sites, it is expected that NO_x stored on them would be reduced faster than that stored on the slow sites, which are further away from the Pt sites. From Fig. 2, it is observed that during the evolution of H_2 in the effluent, the outlet concentration of H_2 does not immediately increase to its inlet concentration of 1500 ppm. A likely reason for the same is that even after H_2 breakthrough, the reduction of stored NO_x is taking place, albeit at a slower rate. As will be shown later, the H_2 concentration fronts in the axial direction are not very steep. These experimental observations justify the use of two different kinds of BaO sites on the catalyst.

The rates of the steps represented by Eqs. (2.7)–(2.12) are given by:

$$R_{v4} = k_4 X_{H_2,wc} c_{BaO}(f) \theta_{Ba(NO_3)_2}(f) \quad (2.13)$$

$$R_{v5} = k_5 X_{H_2,wc} c_{BaO}(s) \theta_{Ba(NO_3)_2}(s) \quad (2.14)$$

$$R_{v6} = k_6 X_{NH_3,wc} c_{BaO}(f) \theta_{Ba(NO_3)_2}(f) \quad (2.15)$$

$$R_{v7} = k_7 X_{NH_3,wc} c_{BaO}(s) \theta_{Ba(NO_3)_2}(s) \quad (2.16)$$

$$R_{v8} = k_{8f} X_{H_2O,wc} c_X \theta_{v,X} - k_{8b} c_X \theta_{H_2O,X} \quad (2.17)$$

$$R_{v9} = k_{9f} X_{NH_3,wc} c_X \theta_{v,X} - k_{9b} c_X \theta_{NH_3,X} \quad (2.18)$$

$$\theta_{H_2O,X} + \theta_{NH_3,X} + \theta_{v,X} = 1 \quad (2.19)$$

The numerical values of fast and slow storage capacities used in simulating the regeneration are the same as those used for the simulation of storage. The axial concentration profile of the nitrates in the monolith channel at the start of regeneration is taken from the predicted nitrate profile at the end of storage (t = 60 s). The values of the rate constants, k_i (i = 4–7), k_{8f}, k_{8b}, k_{9f} and k_{9b} were adjusted to predict the effluent concentration trends and are given in Table 4. The values of kinetic constants for regeneration by H_2 are taken to be the same as those for regeneration by NH_3 ($k_4 = k_6$ and $k_5 = k_7$), since Mulla et al. [3] reported that H_2 and NH_3 were equally effective in reducing the stored NO_x. This would not be the case at lower temperatures (<230 °C), as shown by Clayton et al. [1].

3. Results and discussion

Fig. 2 shows the comparison between model-predicted and experimental effluent concentrations during regeneration. It is observed that the breakthrough times of H_2 and NH_3 are predicted quite well by the model. The time at which the effluent NH_3 concentration achieves a maximum and the peak value are predicted closely. A high affinity of H_2O to the alumina-based washcoat is the likely reason for the delay in its appearance for early regeneration times, which is predicted by the model. The desorption of H_2O results in a slow H_2O concentration transient after the H_2 breakthrough, which is captured by the model. The model also predicts the N_2 concentration profile, except for early regeneration times. This is probably because in the experiments, NO and NO_2 are evolved during early regeneration times [1]. This so-called "NO_x puff" or the production of N_2O are not considered in the present model.

Table 4
Parameter values used in the regeneration simulations.

Parameter	Numerical value
k_4	3×10^3 s^{-1}
k_5	1.8×10^2 s^{-1}
k_6	3×10^3 s^{-1}
k_7	1.8×10^2 s^{-1}
k_{8f}	10^3 s^{-1}
k_{8b}	0.1 s^{-1}
k_{9f}	2×10^3 s^{-1}
k_{9b}	0.4 s^{-1}
c_X	96.7 mol/m^3 washcoat

Table 5
Comparison of model-predicted and experimental H_2 front velocities.

Location along the monolith (cm)	Front velocity (mm/s)	
	Experiment	Model
0–0.25	0.29	0.3
0.25–0.33	0.31	0.27
0.33–0.67	0.35	0.31
0.67–1.0	0.40	0.39
1.0–1.33	0.47	0.46
1.33–2.0	0.79	0.7

The cycling experiments were carried out for different monolith lengths to study its effect on the effluent concentration profiles [1]. The effluent H_2 concentrations for various monolith lengths are shown in Fig. 3(a). It is observed that the H_2 breakthrough time increases with an increase in the monolith length. This is because of the higher amount of NO_x stored on a monolith of higher length. The model-predicted H_2 concentration profiles are shown in Fig. 3(b). It is seen that the trends with respect to the breakthrough time are predicted well by the model. The H_2 front velocities are calculated by the ratio of change in the position of a reference point with change in time, the reference point being the axial position at which 50% H_2 conversion is obtained. A comparison of the experimental and model predicted front velocities are given in Table 5. It is observed that the experimental front velocities increase down the monolith length, which is an indication of a higher concentration of stored NO_x in the front of the monolith. The model effectively captures this trend, except between 0.25 and 0.33 cm. The predicted decrease in the front velocity between 0.25 and 0.33 cm is because of the model predicted axial profile of stored NO_x at the start of regeneration, which after a short maximum decreases down the length of the monolith (Fig. 1(b)).

The effluent NH_3 concentration profiles for various monolith lengths are shown in Fig. 4(a). It is observed that similar to H_2, the NH_3 breakthrough time increases with an increase in the monolith length. In fact, the breakthrough of NH_3 occurs at approximately the same time as H_2 for all the monolith lengths, with NH_3 breakthrough slightly earlier than H_2. The observed delay in NH_3 breakthrough suggests the reaction of NH_3 formed in the front of the reactor with the stored NO_x downstream. This justifies the inclusion of reactions (6) and (7) in the regeneration model, represented by Eqs. (2.9) and (2.10), respectively. The model predicted NH_3 effluent concentrations are shown in Fig. 4(b). It is observed that the model accurately predicts the time at which NH_3 concentration goes through a maximum. However, the model does not predict the decrease in peak NH_3 concentration when the monolith length is changed from 0.33 to 0.67 cm. The reason for this experimental observation is unclear, but could be related to a non-uniformity of catalyst composition in the catalytic monolith.

The experimental and model-predicted effluent N_2 concentrations for various monolith lengths are shown in Fig. 5(a) and (b), respectively. The model predicts the experimental data, except for early regeneration times. As discussed before, the model assumes that all the stored NO_x is converted to NH_3, which could be further reduced to N_2. However, in the experiments, NO, N_2O and NO_2 are evolved during early regeneration times, which are not considered in the present model. Another reason for the lack of N_2 in the effluent for early regeneration times could be the adsorption of NH_3, rendering it unavailable for reaction with the stored NO_x. Hence, NH_3 adsorption on the catalyst is included in the model, which predicts less than stoichiometric values of peak N_2 concentrations for smaller monolith lengths. However, the delay in N_2 at the monolith outlet is not predicted. Simulations were performed to study the effect of neglecting NH_3 adsorption. These simulations predict the evolution of N_2 in the effluent at the stoichiometric concentration (=300 ppm = inlet H_2 concentration/5) at the start of regeneration, i.e., a maximum in the transient N_2 concentration was not predicted, justifying the inclusion of NH_3 adsorption in the model.

It is observed from Fig. 5(a) that the experimentally observed N_2 concentrations are higher than the stoichiometric concentration (=300 ppm), even though the difference is less (maximum N_2 concentration = 333 ppm). The accumulation of NH_3 on the catalyst, followed by its desorption and reaction with the stored NO_x could result in N_2 concentrations which are higher than the stoichiometric values. Another plausible reason is that the stored NO_x is present as nitrites in addition to nitrates; the overall reaction for the regeneration of nitrites is given by $3H_2 + Ba(NO_2)_2 \rightarrow 3H_2O + BaO + N_2$. Hence, an inlet H_2 concentration of 1500 ppm would result in an effluent N_2 concentration of 500 ppm, if all the NO_x stored is in the form of nitrites. However, a maximum N_2 concentration of 333 ppm suggests that nitrites, if present, have a low concentration as compared to nitrates.

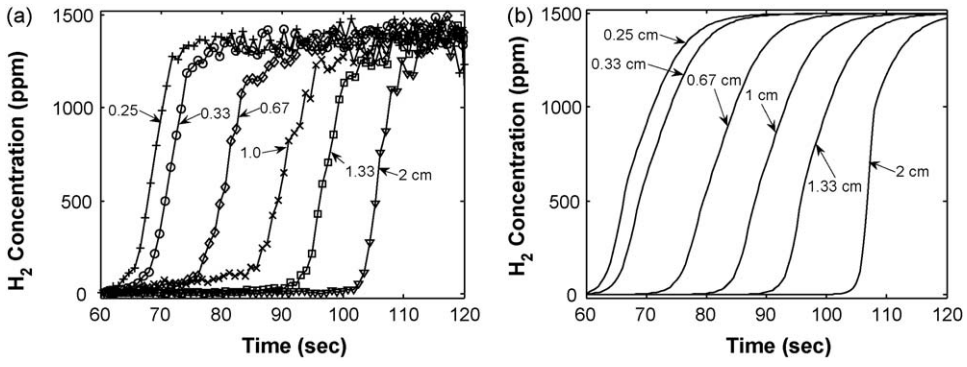

Fig. 3. (a) Experimental and (b) model-predicted effluent H_2 concentrations for various monolith lengths.

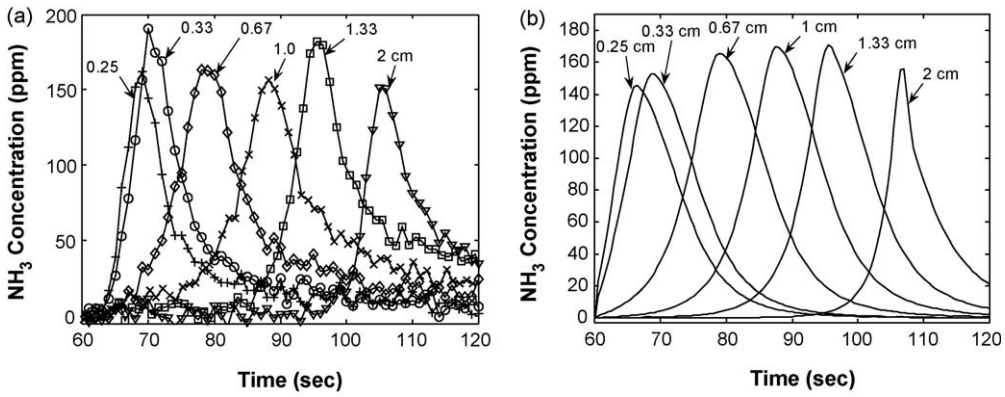

Fig. 4. (a) Experimental and (b) model-predicted effluent NH_3 concentrations for various monolith lengths.

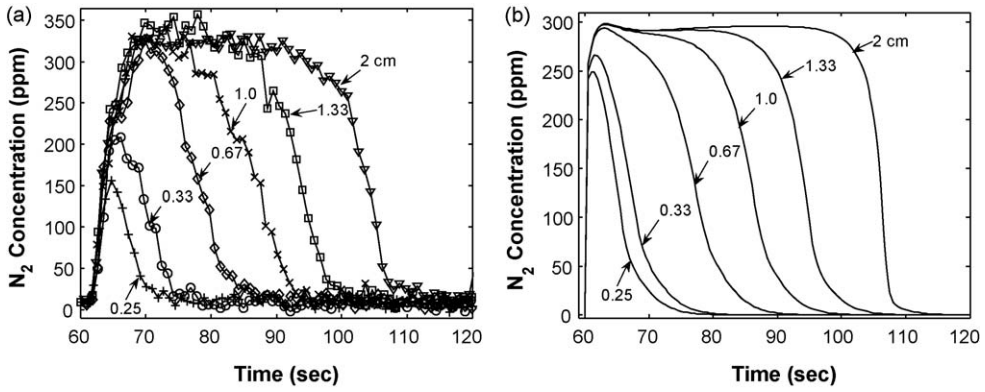

Fig. 5. (a) Experimental and (b) model-predicted effluent N_2 concentrations for various monolith lengths (cm).

The transient data for different monolith lengths was used to study the evolution of spatially propagating fronts of H_2, N_2 and NH_3 at various times during the regeneration [1]. The effluent H_2 concentrations for various monolith lengths are plotted in Fig. 6(a). The results are interpreted such that the effluent concentrations from the various short monolith pieces of lengths, L_i, are considered to be the concentrations at the axial position, L_i, for the longest monolith. It is observed that at the beginning of regeneration, the H_2 concentration decreases sharply to zero from its feed value of 1500 ppm. This is explained by the consumption of H_2 by adsorbed oxygen and stored NO_x, forming a mixture of N_2, N_2O and NH_3. As the regeneration progresses, the H_2 front moves down the reactor because of the depletion of stored NO_x. Fig. 6(b) shows that the model predicts the data quite well. The observed H_2 concentration fronts, even though steep at the beginning of regeneration, are not very steep towards the end of regeneration. This shows the presence of stored NO_x in the front of the reactor which gets regenerated at a low rate. The low rate of regeneration is probably because of the presence of stored NO_x far away from the Pt/BaO interface. Hence, the change in slope of the H_2 concentration fronts with time justifies the use of two different kinds of BaO sites, which differ in their reduction activity. Similar to storage, it was attempted to predict the regeneration behavior using a single type of BaO site. However, the concentration fronts could not be predicted very well, especially the change from the steep H_2 fronts at the start of regeneration to the less steep fronts towards the end of regeneration.

The effluent NH_3 concentration during regeneration for various monolith lengths is shown in Fig. 7(a). It is observed that NH_3

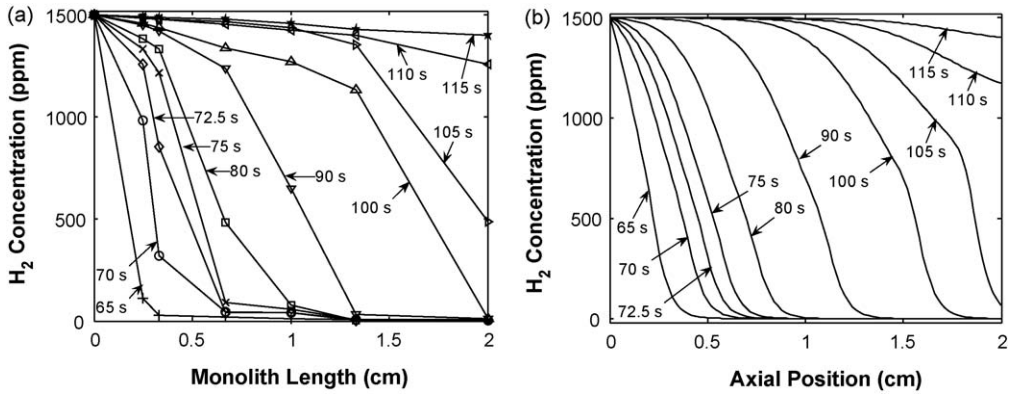

Fig. 6. (a) Effluent H_2 concentration profile for various monolith lengths and (b) model-predicted axial H_2 concentration profile at various times during regeneration.

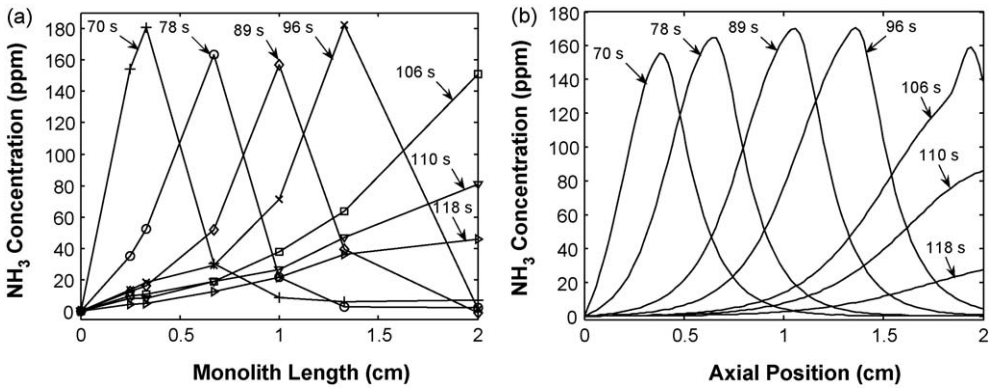

Fig. 7. (a) Effluent NH_3 concentration profile for various monolith lengths and (b) model-predicted axial NH_3 concentration profile at various times during regeneration.

concentration goes through a maximum with axial position, until the breakthrough time, when NH_3 is observed at the outlet of the reactor. Before the breakthrough of H_2 and NH_3 occurs, the NH_3 reduces the stored NO_x downstream of the H_2 front. As the H_2 concentration front reaches the end of the reactor, the NH_3 produced is observed at the outlet. Fig. 7(b) shows the model-predicted NH_3 concentration fronts for various times. It is observed that the model accurately predicts the axial position at which the NH_3 concentration maximum is reached. The slight difference in the model-predicted and experimental peak NH_3 concentrations could be because of the difference in the model-predicted and experimental concentration profile of the stored NO_x in the form of nitrates.

Finally, it is observed experimentally that the NH_3 concentration front leads the H_2 concentration front. This can be explained by the lower diffusivity of NH_3 as compared to H_2. Calculations were performed in which the diffusivity of NH_3 is artificially decreased from its original value. The model predicts that decreasing the NH_3 diffusivity results in increasing the time delay between the appearance of NH_3 and H_2, with NH_3 appearing earlier than H_2. Also, the width of the NH_3 front is higher than the original value. Calculations were also performed in which the diffusivity of NH_3 is artificially increased to higher than that of H_2. The model predicts that H_2 appears in the effluent earlier than NH_3. Hence, it is concluded that the lower diffusivity of NH_3 is responsible for the earlier appearance of NH_3 in the effluent than H_2.

4. Conclusions

A simplified global kinetic model for the NO_x uptake and regeneration is developed and is shown to capture the major spatio-temporal features of the lean NO_x trap reported by Clayton et al. [1]. Two different kinds of BaO sites are proposed to be present on the catalyst, which differ in their storage as well as regeneration kinetics. The two-site model explains the near complete NO_x storage at the start of the storage phase and the slow evolution of NO and NO_2 during later storage times. The two different kinds of sites also explain the change in slope of the H_2 concentration fronts with time. The H_2 concentration front is predicted to accelerate as it travels down the monolith, which is consistent with the experimental studies and show the presence of more stored NO_x in the front of the monolith. The model effectively captures the formation of NH_3 during regeneration and its subsequent consumption by stored NO_x, thus resulting in the "moving pulse" behavior of the NH_3 concentration front.

The present model is based on isothermal anaerobic experiments for a short monolith, while regeneration in commercial NO_x traps takes place in the presence of O_2 resulting in a significant temperature rise. Hence, the spatio-temporal dynamics of the adsorption and temperature fronts play an important role in determining the optimal operating strategies. The length and temperature effects will be considered in a forthcoming manuscript.

Acknowledgement

The work reported was supported by a grant from DOE-NETL (DE-FC26-05NT42630).

References

[1] R.D. Clayton, M.P. Harold, V. Balakotaiah, Appl. Catal., B 84 (2008) 616.
[2] R.D. Clayton, M.P. Harold, V. Balakotaiah, C.Z. Wan, Appl. Catal., B 90 (2009) 662.
[3] S.S. Mulla, S.S. Chaugule, A. Yezerets, N.W. Currier, W.N. Delgass, F.H. Ribeiro, Catal. Today 136 (2008) 136.
[4] A. Guthenke, D. Chatterjee, M. Weibel, B. Krutzsch, P. Koci, M. Marek, I. Nova, E. Tronconi, in: G.B. Marin (Ed.), Advances In Chemical Engineering, vol. 33, AP, 2008, p. 103.
[5] M. Sharma, M.P. Harold, V. Balakotaiah, Ind. Eng. Chem. Res. 44 (2005) 6264.
[6] M. Sharma, M.P. Harold, V. Balakotaiah, SAE J. 2005-01-3882 (2005).
[7] L. Olsson, H. Persson, E. Fridell, M. Skoglundh, B. Andersson, J. Phys. Chem. B 105 (2001) 6895.
[8] W.S. Epling, J.E. Parks, G.C. Campbell, A. Yezerets, N.W. Currier, L.E. Campbell, Catal. Today 96 (2004) 21.
[9] R.L. Muncrief, P. Khanna, K.S. Kabin, M.P. Harold, Catal. Today 98 (2004) 393.
[10] K.S. Kabin, P. Khanna, R.L. Muncrief, V. Medhekar, M. Harold, Catal. Today 114 (2006) 72.
[11] B.R. Kromer, L. Cao, L. Cumaranatunge, S.S. Mulla, J.L. Ratts, A. Yezerets, N.W. Currier, F.H. Ribeiro, W.N. Delgass, J.M. Caruthers, Catal. Today 136 (2008) 93.
[12] U. Tuttlies, V. Schmeisser, G. Eigenberger, Chem. Eng. Sci. 59 (22–23) (2004) 4731.
[13] L. Olsson, R.J. Blint, E. Fridell, Ind. Eng. Chem. Res. 44 (9) (2005) 3021.
[14] P. Koci, F. Plat, J. Stepanek, M. Kubicek, M. Marek, Catal. Today 137 (2008) 253.
[15] L. Cumaranatunge, S.S. Mulla, A. Yezerets, N.W. Currier, W.N. Delgass, F.H. Ribeiro, J. Catal. 246 (1) (2007) 29.
[16] J.A. Pihl, J.E. Parks II, C.S. Daw, T.W. Root, SAE Tech. 2006-01-3441 (2006).
[17] L. Lietti, I. Nova, P. Forzatti, J. Catal. 257 (2008) 270.
[18] R.S. Larson, J.A. Pihl, V.K. Chakravarthy, T.J. Toops, C.S. Daw, Catal. Today 136 (2008) 104.
[19] J. Xu, M.P. Harold, V. Balakotaiah, Appl. Catal., B 89 (1–2) (2009) 73.
[20] A. Lindholm, N.W. Currier, J. Li, A. Yezerets, L. Olsson, J. Catal. 258 (2008) 273.
[21] K. Ramanathan, V. Balakotaiah, D.H. West, Chem. Eng. Sci. 58 (2003) 1381.
[22] D. Bhatia, M.P. Harold, V. Balakotaiah, Chem. Eng. Sci. 64 (2009) 1544.
[23] S. Erkfeldt, E. Jobson, M. Larrson, Top. Catal. 16/17 (1–4) (2001) 127.
[24] D. Bhatia, R.W. McCabe, M.P. Harold, V. Balakotaiah, doi:10.1016/j.jcat.2009.05.020.
[25] I. Nova, L. Castoldi, L. Lietti, E. Tronconi, P. Forzatti, F. Prinetto, G. Ghiotti, J. Catal. 222 (2002) 377.